Simulation and Measurement of Electromagnetic Wave Propagations along a Wearable E-Textile Metasurface Transmission Line

Jose Alcala-Medel*, Jayshri Kulkarni, Stephen McClain and Yang Li
School of Engineering and Computer Science, Baylor University, Waco TX 76798, U.S.A.

***Abstract* —** This study introduces a compact wearable metasurface transmission line operating at 2.45 GHz, utilizing spoof surface plasmon polariton (SSPP). The design incorporates a periodic arrangement of hook unit cells and a tapering structure to enhance coupling efficiency between the microstrip feed line and the metasurface transmission line. For its implementation, a dielectric substrate composed entirely of cotton denim jeans is employed, along with e-textile conductive traces and a ground plane. Electromagnetic wave propagation along the transmission line is simulated, and the primary wave mode and associated propagation characteristics are analyzed. Both simulation and measurement results confirm the successful performance of the metasurface transmission line for on-body signal transmissions.

Index Terms — Metasurface, Spoof surface plasmon polariton (SSPP), Body area network (BAN), E-textile, Wearable, Transmission Line

I. INTRODUCTION

In the past decade, wearable smart devices have transitioned from being a novel technology to becoming an indispensable tool for day-to-day activities, and this transformation has sparked a growing demand for wireless body area networks (WBAN). Given that these networks confront challenges like increasing energy consumption and heightened spectral demand, establishing robust and power-efficient wireless connections between these devices is imperative. Prior research has endeavored to address challenges associated with on-body signal transmission at the physical layer level by leveraging the communication protocols specified in the IEEE 802.15.6 WBAN standard. This standard outlines three distinct signal transmission mechanisms in proximity to a human subject: Intrabody communication, Narrowband, and Ultrawideband [1].

The intrabody communication operates within the lowest spectrum, specifically below 100 MHz, thereby providing a more private and power-efficient operation due to its use of the human body as the transmission medium, as opposed to conventional radiating antennas [1-3]. Nevertheless, the implementation of intrabody communication introduces its own unique set of challenges, primarily centered around the necessity of employing coupling electrodes. Furthermore, the human body channel is plagued by relatively high signal attenuation and limited bandwidth. Research has also delved into the use of narrowband and ultrawideband specifications to harness the space wave (line-of-sight) or creeping wave (non-line-of-sight) phenomena [4, 5]. However, the propagation of electromagnetic (EM) waves on the human body surface gives rise to challenges, including high transmission loss and susceptibility to the motion of the human body. Furthermore, on-body antennas emit EM waves into

the surrounding space, which introduces complexities in safeguarding the privacy of sensitive information, such as health data.

A more secure and less lossy approach to propagating RF signals around the human body can be implemented by integrating a guided transmission line with clothing. Prior research has explored the use of wearable magnetic inductive waveguides [6, 7], or flexible waveguide/e-textile connections [8] to enhance on-body signal transmission, primarily operating within the HF/VHF bands below 100 MHz and having limited bandwidth. In a recent study [9, 10], a novel wearable transmission line based on spoof surface plasmon polariton (SSPP) was introduced and implemented. This design leverages the slow wave propagation occurring at the dielectric-metal boundary to confine wave propagation along the transmission line, resulting in superior performance regarding signal transmission loss and privacy. However, achieving a cutoff frequency near 2.40 GHz requires the SSPP unit cell to have a relatively large size [9, 10, 11] or to lack the necessary shielding and flexibility to aid in transmission on the human body [12-17]. It is also notable that in these previous works, the electromagnetic wave propagation characteristics (i.e., propagation constants, attenuation constants, and field distributions) of the dominant mode along the wearable transmission line were not extracted.

In this paper, we introduce a compact design for an e-textile metasurface transmission line for application in wearable technology. The electromagnetic wave propagations along the wearable transmission line are simulated and its dominant wave mode characteristics are extracted. Furthermore, we implement and measure the metasurface transmission line design using a unique e-textile fabrication technique, facilitating the seamless integration of electronics into clothes. This paper is organized as follows: Section II presents the theory and simulation related to the wearable metasurface transmission line. Section III extracts and verifies the wave propagation characteristics of the dominant mode. Section IV provides details on the fabrication process and measurement results. Finally, Section V concludes the paper.

II. DESIGN AND SIMULATION

Figure 1 (a) illustrates the unit cell design of the metasurface transmission line, which adopts a hook-shaped configuration. The hook-shaped unit cell design facilitates the cancellation of the tangential component of the electrical field, as induced currents in the hook follow a circular pattern. This results in an electrical field with a predominantly normal component (E_z), leading to the emergence of an evanescent mode and confined propagation along the transmission line in the x-direction, as shown in Figure 1 (b). The dimensions (‘a’ and ‘h’) and period (‘p’) of the pattern are at the sub-wavelength scale and carefully selected to induce an SSPP mode that exhibits strong interaction with incoming EM waves. A perfect electrical conductor (PEC) serves as the conductive material, and the dielectric substrate consists of denim with $\varepsilon_r = 1.93$ and a thickness of 0.8 mm. A PEC ground plane is positioned behind the denim, providing shielding against the human body's lossy tissues. The values of 'a' and 'p' are set at 2 mm and 6 mm, respectively, with the height 'h' being adjustable to modify the cut-off frequency of the propagating modes.

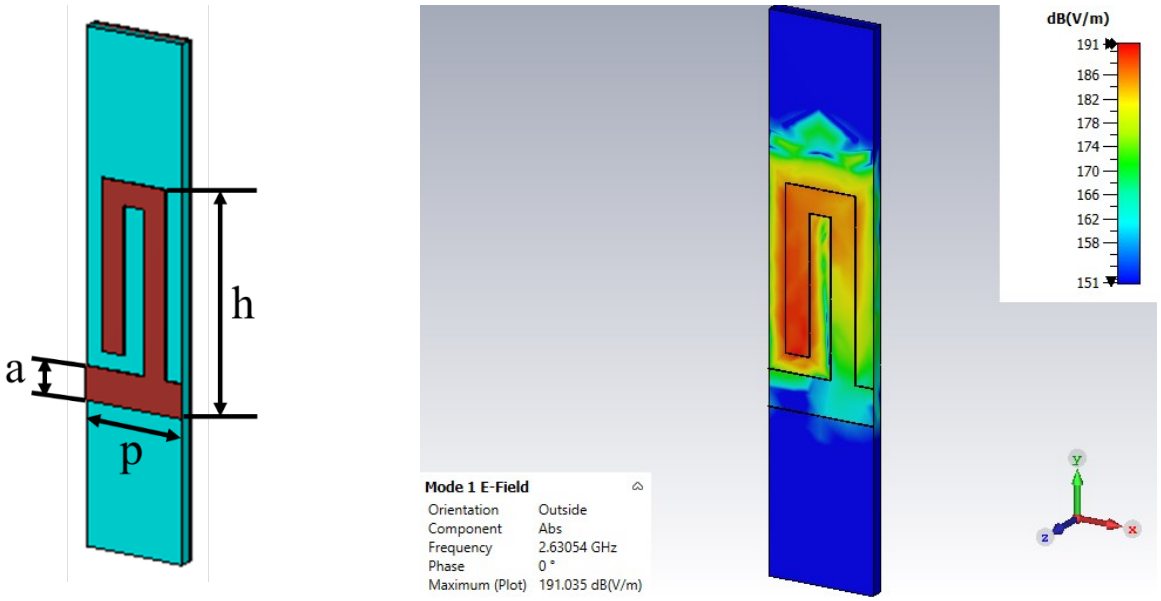

Figure 1. (a) Unit hook cell design (b) Simulated near electrical field E_z strength on the transmission line unit cell structure.

To characterize the design, we conducted simulations of the dispersion diagram for an infinitely long transmission line using the eigenmode solver in CST Microwave Studio with a periodic boundary condition. In Figure 2, we present the dispersion diagram simulated with CST for various heights of the unit cell hook.

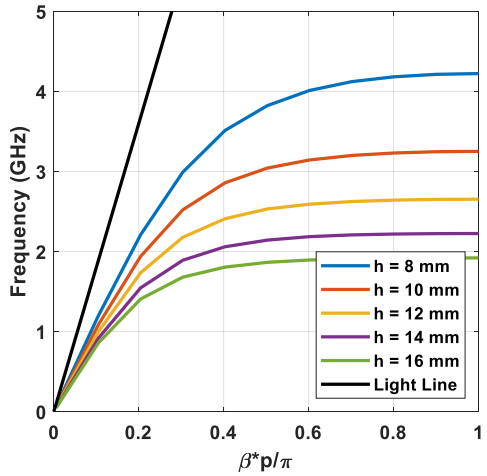

Figure 2. Dispersion diagrams for various values of height *h*

The simulation results confirm the occurrence of slow wave propagation along the infinite metasurface transmission line, where the propagation constants exceed those of free space, as indicated by the light

line. As the height h increases, the cut-off frequency, at which the asymptotic line appears, decreases. The cut-off frequencies of the wave mode are observed to align closely when h is approximately equal to $\frac{\lambda_o}{10}$. Furthermore, as the operating frequency approaches the cut-off frequency, the propagation constant β along the x dimension rapidly increases, leading to quicker field decay in the direction normal to the propagation. In our design, we have optimized the performance of our wearable transmission line by having chosen a unit cell height h of 12 mm, placing the operating frequency of 2.45 GHz below, yet proximate to, the cut-off frequency to confine the wave propagation.

Next, we simulate a finite-length metasurface transmission line. Figure 3 depicts a 5-element transmission line design. To efficiently feed the transmission line, gradient hook sections are employed to match the phase velocity of the transmission line with that of a microstrip feed line. This tapering feeding technique effectively mitigates significant reflection loss and minimizes the reduction in bandwidth compared to using a feed dipole [9]. The finite transmission line is modeled using a copper trace on a denim dielectric with $\varepsilon_r = 1.93$ and a loss tangent of 0.066 defined at 2.45 GHz. The unit cell sizes are identical to those of the infinite-length transmission line, with h set at 12 mm.

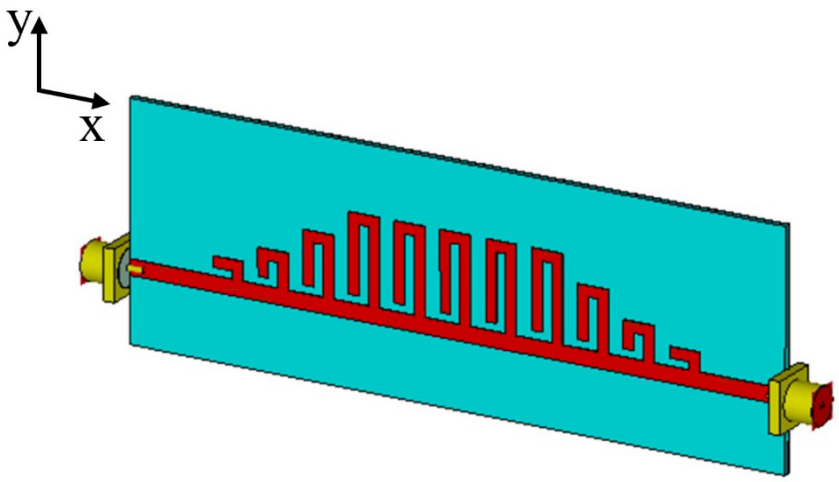

Figure 3. Finite length metasurface transmission line simulation setup.

The simulated S parameters of the finite transmission line are presented in Figure 4, with the frequency ranging from 0-5 GHz. The reflection coefficients can be seen to be below -10 dB across the 2.1 to 2.5 GHz range, indicating that the transmission line is matched within the targeted ISM band. As observed in the transmission data S_{21}, a sharp cutoff occurs near 2.4 GHz, resembling the cutoff frequency observed in the simulation of the infinitely long transmission line in Figure 2. Below the cutoff frequency, the insertion loss within the pass band is above -8 dB, which is much less than the wireless on-body propagation over the same distance, making it ideal for on-body signal transmission. Although the insertion loss is smaller at the lower frequencies, it is preferred to operate the transmission line as close to the cut-off frequency to maximize the wave number along the transmission line, which can result in faster field attenuation away from the transmission line in the normal direction. To illustrate

this, the electric field distributions on the structure within the passband at 2.1 GHz are simulated and depicted in Figures 5(a) and (b).

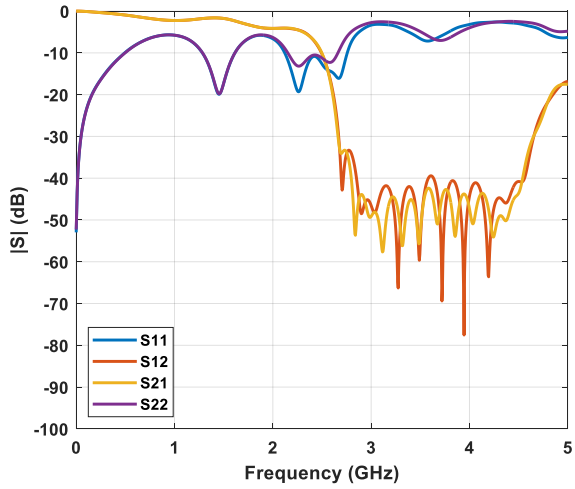

Figure 4. S-parameter simulation results for the 5-element finite length transmission line.

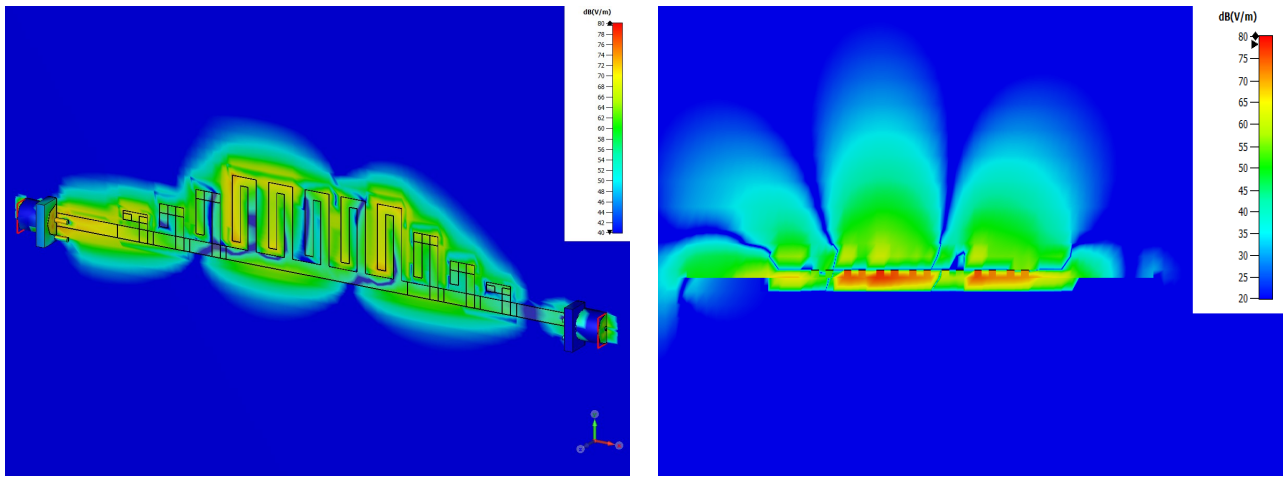

(a) (b)

Figure 5. Electric field distribution on the transmission line at 2.1 GHz. (a) The total E-field on transmission line surface. (b) the z component of the E-field on the xz plane. Propagation of wave along x direction.

In Figure 5(a), the highest field intensity occurs between the hooks of the unit cell, with the field rapidly attenuating as distance increases from the hooks. Figure 5(b) illustrates the z component of the electric field, perpendicular to the boundary of the conducting metal and the air, indicating the presence of an evanescent mode component that diminishes exponentially away from the transmission line's surface. These observations suggest that the fields are predominantly confined within the transmission line structure, resulting in minimal signal leakage and interference with neighboring transmission lines. This characteristic makes it well-suited for privacy-sensitive wearable applications.

Moreover, figure 5(b) demonstrates a minimal to negligible electric field beneath the structure on the opposite side of the ground plane. This feature offers significant advantages for the operation of the transmission line in wearable applications, effectively shielding it from the body's lossy tissues.

The impact of the human body and the bending effects on the performance of the transmission line have also been simulated. Figure 6 shows the transmission line wrapped around a cylinder of lossy muscle that represents the human arm.

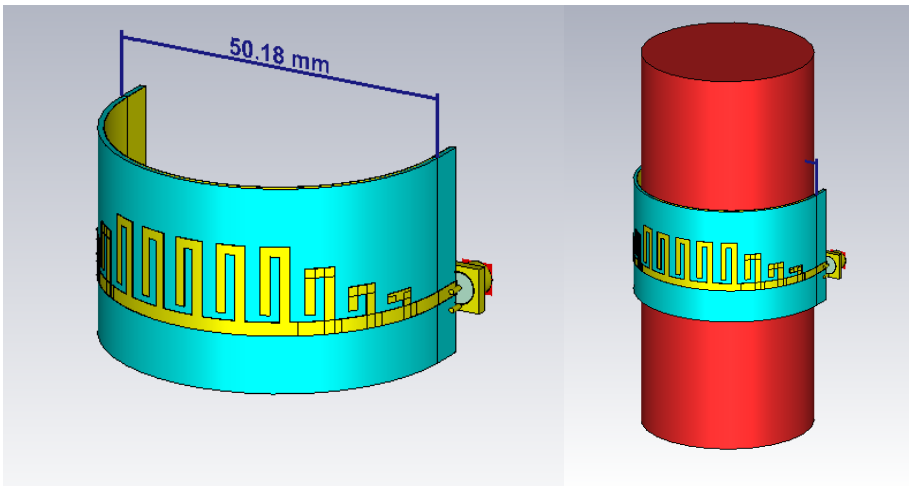

(a) (b)

Figure 6. The proposed metasurface transmission line wrapped around (a) air and (b) a cylinder filled with muscle

Figure 7 compares the simulated S11 and S21 for three cases: flat transmission line in the air, bent transmission line in the air, and bent transmission line around the lossy muscle cylinder. The results are similar to each other in all three cases, implying that the designed transmission line operates well for wearable applications.

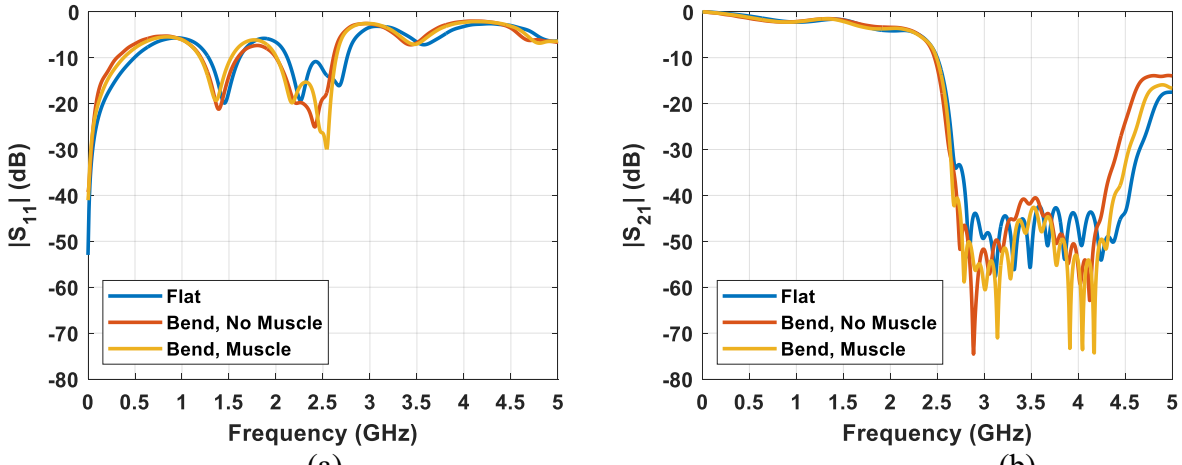

(a) (b)

Figure 7. The simulated S-parameters of the proposed wearable metasurface transmission line: (a) S11 and (b) S21

III. EXTRACTION OF DOMINANT MODE USING ESPRIT ALGORITHM

To identify the dominant propagation mode along the transmission line, we analyze the simulated electric field at each frequency by modeling it as a superposition of wave modes. Each mode is characterized by its unique field strength C_n, propagation constant β_n, and attenuation constant α_n, as expressed in Eq. (1) below. Subsequently, we employ the Estimation of Signal Parameters via Rotational Invariant Techniques (ESPRIT) algorithm to extract the signal parameters from the simulated electric field along the transmission line. Originally developed for direction of arrival finding [18], ESPRIT has been successfully adapted for antenna radiation and wave propagation problems [19, 20]. By applying ESPRIT individually to each frequency within the passband, we effectively extract the dominant mode (i.e., the one with the largest C_n) along with its associated propagation and attenuation constants below the cut-off frequencies.

$$E(x,y) = \sum_n c_n(y) e^{-j\beta_n x} e^{-\alpha_n x} \tag{1}$$

The motivation for using the ESPRIT algorithm in this work consists of three primary reasons. Firstly, the algorithm enables the extraction of wave parameters for the proposed transmission line by sampling the coupled E-field of a single transmission line sample. Secondly, the algorithm can also extract the dominant modes of the structure offering insights into the fields propagating on the structure. Lastly, the algorithm can extract the wave parameters for structures exhibiting nonlinear phase characteristics, such as 2-D SSPP transmission lines. These attributes make the ESPRIT algorithm a robust tool for the analysis of SSPP transmission lines.

To validate the results obtained from the ESPRIT extraction, we also extracted the propagation and attenuation constants of the transmission line from the S-parameters using the method proposed in [21]. Initially, the S-parameters of two transmission line samples, one with N elements and the other with N+1 elements, are simulated using CST. In our investigation, the 5-element transmission line is designated as the N element sample, while a 6-element transmission line is simulated to represent the N+1 element sample. Subsequently, we apply the following equations, originally presented in the paper by Zhang et al. [21], to calculate the propagation constant of the periodic structure:

$$\gamma = \frac{1}{d}\ln\left(\frac{1}{2}\frac{1}{s_{21}^{(1)}s_{12}^{(2)}}\left[Y \pm \sqrt{Y^2 - 4s_{12}^{(1)}s_{21}^{(1)}s_{12}^{(2)}s_{21}^{(2)}}\right]\right) \tag{2}$$

$$Y = -s_{11}^{(1)}s_{22}^{(1)} + s_{12}^{(1)}s_{21}^{(1)} + s_{11}^{(1)}s_{22}^{(2)} + s_{22}^{(1)}s_{11}^{(2)} - s_{11}^{(2)}s_{22}^{(2)} + s_{12}^{(2)}s_{22}^{(2)} \tag{3}$$

Where $s_{i,j}^{(n)}$ are the S-parameters of sample n, d is the periodic length of the unit cell, and γ is the complex propagation constant of the transmission line. Using these equations, we are able to find the attenuation constant and wave number of the transmission line by taking the real and imaginary parts of the propagation constant respectively.

Figures 8 (a) and (b) depict the extracted propagation and attenuation constants obtained from both the ESPRIT and S-parameter approaches. The two sets of results exhibit excellent agreement, demonstrating a rapid increase in both propagation and attenuation constants as the frequency approaches the cut-off frequency. Additionally, we have included the results of the dispersion calculations from the infinitely long structure, computed using the CST eigen solver, for comparison. The trends are very similar, and any minor discrepancies can be attributed to the finite versus infinite nature of the structure.

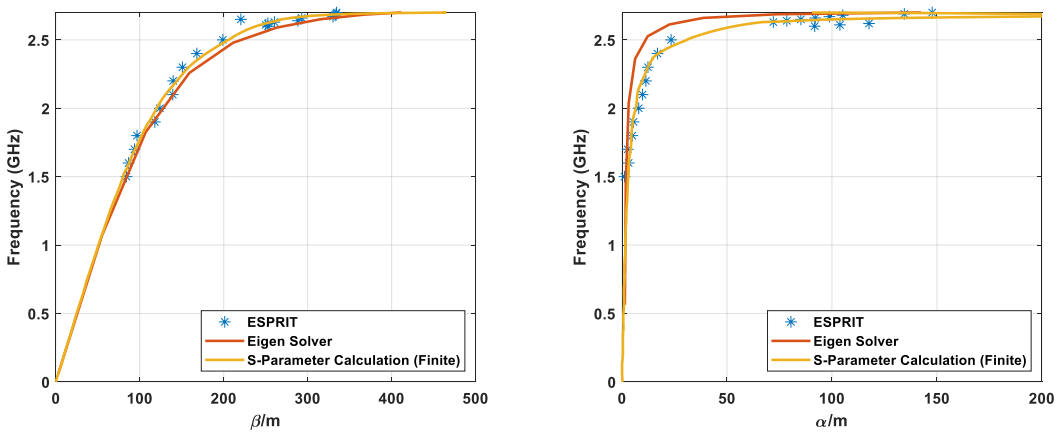

Figure 8. Extracted wave mode characteristics: (a) propagation constants (b) attenuation constants.

The ESPRIT method also enables the determination of the amplitude of the dominant mode component C_n at various heights Y along the transmission line structure. Figures 9 (a) and (b) illustrate the normalized E_z and E_y components extracted from ESPRIT, comparing them with the CST simulated electric field distributions. The two sets of results exhibit good agreement, primarily due to the significantly weaker amplitudes of higher-order modes. The conductive traces of the SSPP transmission line are situated within the coordinates Y = 0 mm to Y = 13 mm, while the denim material extends from Y = -8.2 mm to Y = 21.5 mm. Outside the conductive trace, the extracted mode field demonstrates rapid exponential decay in both positive and negative Y-directions, consistent with the observations in Figure 5 (a). Within the conductive trace, the field exhibits rapid variation, with both E_z and E_y field strengths reaching maximum values near the top of the hook.

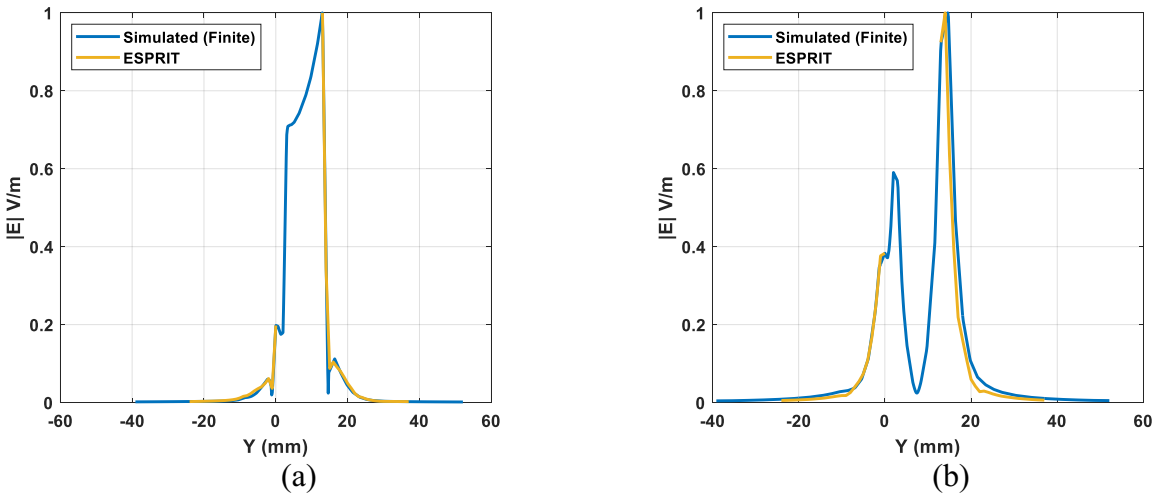

Figure 9. Comparison of the normalized e-field generated using the CST simulation and the ESPRIT algorithm for the (a) E_z component and (b) E_y component.

IV. Fabrication and Measurement

To validate the simulation results, a prototype of the metasurface transmission line was fabricated using an Epilog Fusion Edge 36 60-watt laser cutter and the following materials: A nickel-copper coated polyester to serve as the conductive fabric, 12 oz denim for the substrate, 725PLKG Heavy Duty Wonder Under fusible web, copper tape and 41 mil SMA connectors.

The fabrication procedure proceeds as follows: first, the conductive material is affixed to both sides of the denim substrate. Subsequently, utilizing the laser cutter, the transmission line pattern is engraved into one side of the denim substrate, exclusively cutting the conductive fabric while preserving the denim material. After the pattern is cut out, surplus conductive fabric is removed, leaving only the transmission line pattern intact. Copper tape is then utilized to attach the SMA connectors to the transmission line ports. Finally, continuity checks are performed to verify the integrity of the conductive fabric and ensure continuity between the SMA connectors' grounds.

Figure 10 showcases the top and bottom views of the final fabricated prototype. The dimensions of the completed prototype measure 9×3×0.1 cm^3. Subsequently, the S-parameters of the transmission line were measured using a VNA, with the frequency swept from 300 kHz to 5 GHz.

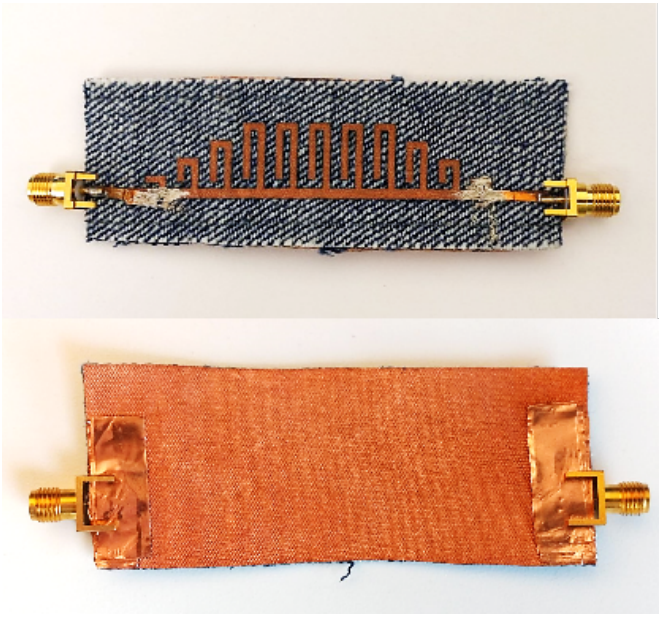

Figure 10. Fabricated prototype metasurface transmission line top and bottom.

Figure 11 illustrates a comparison between the measured and simulated S-parameters of the transmission line. The results exhibit a notable agreement between the simulated and measured reflection and transmission data, with both cutoff frequencies occurring close to 2.5 GHz. The low insertion loss within the passband suggests that the transmission line can effectively transmit over the frequencies of interest with minimal loss. Any discrepancies between the simulation and measurement can likely be attributed to fabrication errors and the utilization of a constant dielectric constant for denim in our simulation.

The propagation and attenuation constants of the transmission line were also computed from the measured S-parameters and compared with their simulation counterparts in the previous section. Figure 12 presents the calculated dispersion and attenuation curves for the fabricated transmission line prototypes. The figures illustrate a reasonable agreement between the simulated and measured dispersion and attenuation results.

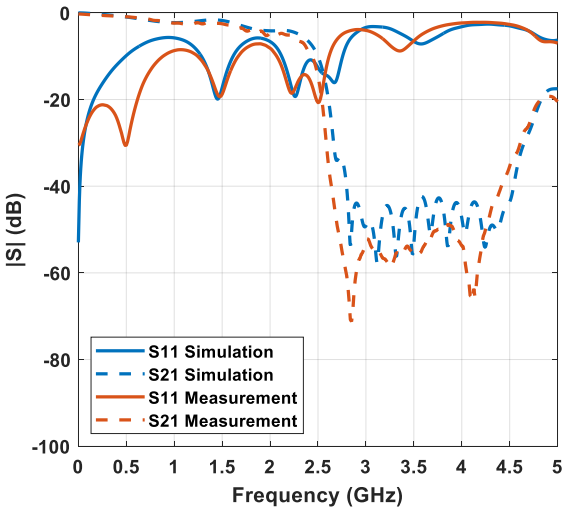

Figure 11. Comparison of S_{11} and S_{21} for the simulated and measured metasurface transmission line.

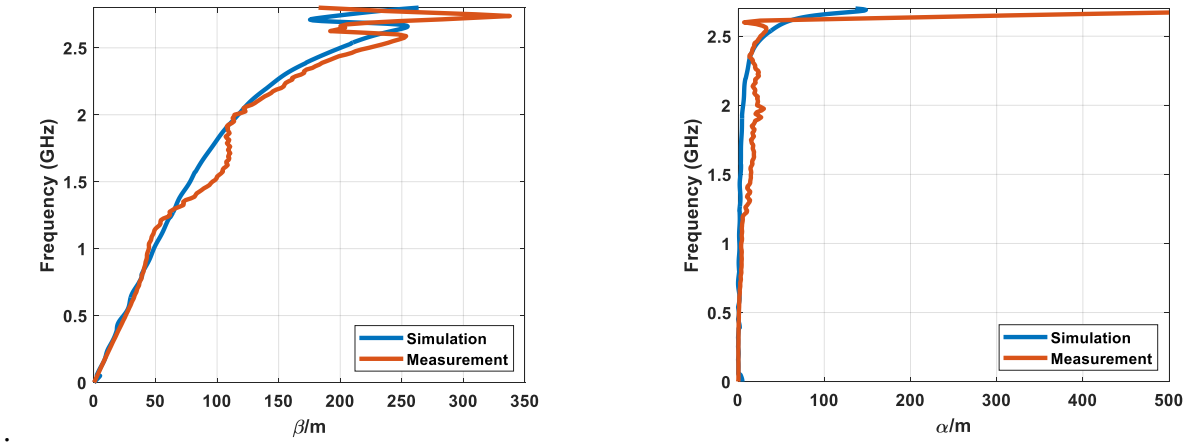

Figure 12. Comparison between simulated and measured results of the (a) propagation constants and (b) attenuation constants.

Finally, we examined the impact of the human body and the bending effects on the performance of the transmission line. The prototype was positioned on the wrist of a test subject, as depicted in Figure 13. Figure 14 presents comparisons of S_{21} for the transmission line when wrapped around cylinders of varying sizes, as well as when placed on the wrist. The graph clearly indicates that bending the metasurface transmission line prototype had no significant impact on its performance within the passband. The transmission curve remains nearly identical under all measurement conditions. These findings also hold true for the transmission line when placed on the human wrist. The demonstrated robustness of the transmission line is promising for wearable applications, as such systems must withstand the natural bends and lossy characteristics of the human body.

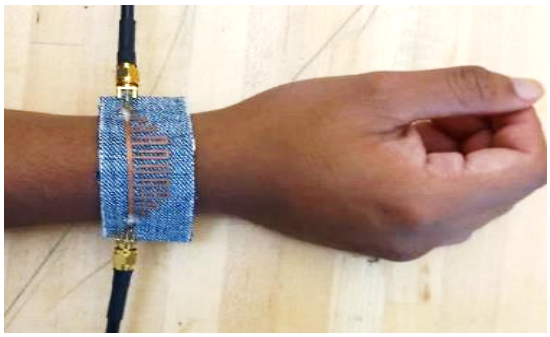

Figure 13. Measurement setup for the SSPP transmission line prototype on human wrist

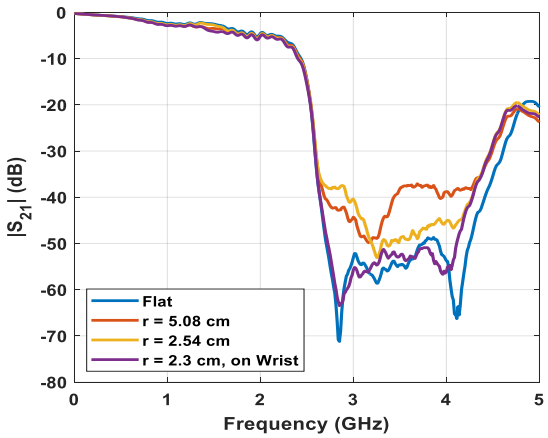

Figure 14. Comparison of S_{21} for the SSPP transmission line when wrapped around cylinders of varying size as well as when placed on the wrist.

V. CONCLUSION

This study presents a tailored design of a compact e-textile metasurface transmission line for wearable applications. The research began with simulations of the propagation characteristics of an infinitely long transmission line, including analysis of the propagation constant and modal field distributions. Following this, a finite-length transmission line prototype was developed, incorporating a tapering feeding structure. Analysis revealed the extraction of the dominant wave mode, demonstrating strong agreement between simulation and measurement in its propagation characteristics.

Four key findings have emerged from this research work: Firstly, the proposed unit cell hook design can be easily adjusted to accommodate different cut-off frequencies, giving the freedom of control of electromagnetic wave propagations along it. Secondly, the ESPRIT algorithm has been successfully introduced to extract the dominant wave mode and its associated propagation constants, attenuation constants, and mode distributions. Thirdly, the design was implemented using a unique e-textile fabrication technique which can also shield the radiation from the lossy body tissue thanks to the ground plane. Lastly, the on-body and bending test have confirmed the usefulness of the transmission line for

wearable applications. For future work, the metasurface transmission line will be integrated with wearable antennas for communication and sensing purposes.

REFERENCES

[1] S. A. Salehi, M. A. Razzaque, I. Tomeo-Reyes and N. Hussain, "IEEE 802.15.6 standard in wireless body area networks from a healthcare point of view," *2016 22nd Asia-Pacific Conference on Communications (APCC)*, Yogyakarta, 2016, pp. 523-528.

[2] M. A. Callejón, D. Naranjo-Hernández, J. Reina-Tosina and L. M. Roa, "A Comprehensive Study Into Intrabody Communication Measurements," *IEEE Transactions on Instrumentation and Measurement*, vol. 62, no. 9, pp. 2446-2455, Sept. 2013.

[3] Ž. Lucev, I. Krois and M. Cifrek, "A Capacitive Intrabody Communication Channel from 100 kHz to 100 MHz," *IEEE Transactions on Instrumentation and Measurement*, vol. 61, no. 12, pp. 3280-3289, Dec. 2012

[4] E. George and C. Saha, "Investigation of Creeping Wave Characteristics Using Cross-Slot Antenna on 12-Cylinder Phantom Model," *IEEE Antennas and Wireless Propagation Letters*, vol. 21, no. 10, pp. 2090-2094, Oct. 2022, doi: 10.1109/LAWP.2022.3190919.

[5] D. Bresnahan and Y. Li, "Investigation of Creeping Wave Propagation Around the Human Head at ISM Frequencies," *IEEE Antennas and Wireless Propagation Letters*, vol. 16, pp. 2767-2770, 2017, doi: 10.1109/LAWP.2017.2745461.

[6] V. Mishra and A. Kiourti, "Wearable Magnetoinductive Waveguide for Low-Loss Wireless Body Area Networks," *IEEE Transactions on Antennas and Propagation*, vol. 69, no. 5, pp. 2864-2876, May 2021, doi: 10.1109/TAP.2020.3030987.

[7] V. Mishra and A. Kiourti, "Wearable Planar Magnetoinductive Waveguide: A Low-Loss Approach to WBANs," *IEEE Transactions on Antennas and Propagation*, vol. 69, no. 11, pp. 7278-7289, Nov. 2021, doi: 10.1109/TAP.2021.3070681.

[8] T. T. Lan, Y. Shinozaki, T. Okura and H. Arai, "A Free-Access Segmented Coplanar Waveguide for On-Body Communication," *IEEE Transactions on Antennas and Propagation,* vol. 66, no. 9, pp. 4524-4532, Sept. 2018, doi: 10.1109/TAP.2018.2842302.

[9] X. Tian, M. Zhang and J. S. Ho, "Robust and High-Efficiency Wireless Body Area Networks with Spoof Surface Plasmons on Clothing," 2019 IEEE MTT-S International Microwave Symposium (IMS), Boston, MA, USA, 2019, pp. 1507-1510, doi: 10.1109/MWSYM.2019.8700804.

[10] X. Tian, Q. Zeng, D. Nikolayev and J. S. Ho, "Conformal Propagation and Near-Omnidirectional Radiation With Surface Plasmonic Clothing," *IEEE Transactions on Antennas and Propagation*, vol. 68, no. 11, pp. 7309-7319, Nov. 2020, doi: 10.1109/TAP.2020.2998216.

[11] A. Ghaddar, B. Garnier, F. Rault, E. Lheurette, L. Burgnies, "Wearable Spoof Surface Plasmon Polariton Transmission Line," E3S Web of Conferences. 351, 2022 10.1051/e3sconf/202235101090.

[12] H. Wan and B. Pan, "A Compact Multi-layer Structure Based on Spiral Spoof Surface Plasmon Polaritons with High Efficiency of High-order Modes," 2023 International Applied Computational Electromagnetics Society Symposium (ACES-China), Hangzhou, China, 2023, pp. 1-3, doi: 10.23919/ACES-China60289.2023.10249768.

[13] W. T. Zhu, B. C. Pan and G. Q. Luo, "Compact design of complementary spoof surface plasmon polaritons transmission line," 2019 IEEE International Symposium on Radio-Frequency Integration Technology (RFIT), Nanjing, China, 2019, pp. 1-3, doi: 10.1109/RFIT.2019.8929210.

[14] B. C. Pan, G. Q. Lou, Z. Liao, J.L. Cai, and B. G. Cai, “Wideband Miniaturized Design of Complementary Spoof Surface Plasmon Polaritons Waveguide Based on Interdigital Structures,” in Scientific Reports vol. 10, 3258 Feb. 2020. doi: 10.1038/s41598-020-60244-7

[15] Wan, Y., Wang, X. H., & Wang, Y. C. (2019). A planar strongly confined spoof surface plasmonic waveguide with compact cells. *Journal of Electromagnetic Waves and Applications*, *33*(12), 1652–1659. https://doi.org/10.1080/09205071.2019.1627250

[16] Shen, S., Xue, B., Shi, M., & Xu, J. (2019). Odd-mode and even-mode SSPPs transmissions based on complementary comb-like structure. Journal of Electromagnetic Waves and Applications, 33(18), 2499–2512. https://doi.org/10.1080/09205071.2019.1687337

[17] Anwar, R. S., Wei, Y., Mao, L., Li, X., & Ning, H. (2019). Novel spoof surface plasmon polaritons on a planar metallic strip with periodic semi-elliptical grooves at microwave frequency. Journal of Electromagnetic Waves and Applications, 33(2), 125–137. https://doi.org/10.1080/09205071.2018.1529631

[18] A. Paulraj, R. Roy and T. Kailath, "Estimation Of Signal Parameters Via Rotational Invariance Techniques- Esprit," Nineteeth Asilomar Conference on Circuits, Systems and Computers, 1985., Pacific Grove, CA, USA, 1985, pp. 83-89, doi: 10.1109/ACSSC.1985.671426.

[19] Y. Li and H. Ling, “Improved current decomposition in helical antennas using the ESPRIT algorithm,” *Progress in Electromag. Research*, vol. 106, pp. 279-293, July 2010.

[20] Y. Li, “Wave propagation along a one-dimensional metal cut-wire array,” *Journal of Electromagnetic Waves and Applications*, vol. 27, no. 1, pp. 3-13, Jan. 2013

[21] L. P. Zhang, H. C. Zhang, Z. Gao and T. J. Cui, "Measurement Method of Dispersion Curves for Spoof Surface Plasmon Polaritons," *IEEE Transactions on Antennas and Propagation*, vol. 67, no. 7, pp. 4920-4923, July 2019, doi: 10.1109/TAP.2019.2916645.